Amorphous silica nanoparticles accelerated atherosclerotic lesion progression in ApoE-/- mice through endoplasmic reticulum stress-mediated CD36 up-regulation in macrophage

Ru Ma
Capital Medical University
Yi Qi
Capital Medical University
Xinying Zhao
Capital Medical University
Xueyan Li
Capital Medical University
Xuejing Sun
Capital Medical University
Piye Niu
Capital Medical University
Yanbo Li
Capital Medical University
Caixia Guo (guocx@ccmu.edu.cn)
Capital Medical University https://orcid.org/0000-0002-5207-8059
Rui Chen
Capital Medical University
Zhiwei Sun
Capital Medical University

Research

Keywords: Silica nanoparticles, atherosclerosis, foam cell, endoplasmic reticulum stress, CD36

Posted Date: May 12th, 2020

DOI: https://doi.org/10.21203/rs.3.rs-26885/v1

Version of Record: A version of this preprint was published on October 2nd, 2020. See the published version at https://doi.org/10.1186/s12989-020-00380-0.

Abstract

Background

Given the prominent cardiovascular effects of nanosized particulate matter in air pollution, our limited understanding of the potential cardiovascular effects of engineered nanoparticles, in particular, is a pressing concern. Silica nanoparticles (SiNPs) are among the most widely manufactured and used nanoparticles. However, the interaction between SiNPs exposure and atherosclerosis, and the underlying mechanisms still remain unknown.

Results

Ultrasound microscopy showed a significant increase of pulse wave velocity (PWV) in ApoE$^{-/-}$ mice fed by a Western diet after SiNPs exposure *via* intratracheal instillation compared to the control mice. Histopathological investigation reflected a greater plaque burden with higher lipid load in the aortic root of SiNPs-exposed ApoE$^{-/-}$ mice. When compared to the control, serum levels of total triglycerides (TG) and low-density lipoprotein cholesterol (LDL-C) were significantly elevated after SiNPs exposure. Moreover, intensified macrophage infiltration and endoplasmic reticulum (ER) stress were occurred in plaques after SiNPs exposure, as evidenced by the upregulated CD68 and Bip, CHOP levels. Further, in vitro, SiNPs was confirmed to activate ER stress and induce lipid accumulation in mouse macrophage, RAW264.7. Mechanistic analyses showed that 4-PBA (a classic ER stress inhibitor) pretreatment could greatly alleviate SiNPs-induced macrophage lipid accumulation, and reverse the elevated CD36 expression by SiNPs.

Conclusions

Our results firstly revealed the acceleratory effect of SiNPs on atherosclerosis in ApoE$^{-/-}$ mice. SiNPs aggravated the plaque load in the aorta of mice, promoted macrophage infiltration and ER stress inside the lesion, alongside with the exacerbated arterial stiffness and dyslipidemia. Further, ER stress-mediated CD36 upregulation contributed to the formation of macrophage-derived foam cell caused by SiNPs, ultimately contributing to the progression of atherosclerotic plaque.

Introduction

The rapid development and enormous progress in nanotechnology bring the toxicological concerns to nanomaterials (NMs), which might pose potential threats to human health and the environment. Silica nanoparticles (SiNPs) ranked in the top two global producers of nanomaterials, with an annual output of nearly 1.5 million tons [1]. It has a wide range of applications for industrial products and consumers, such as food additive, surfactants, catalysts, sensors, ceramics, paints and solar cells, which also applied in medical and biomedical fields for drug delivery, disease diagnosis and treatment, etc [2, 3]. Such mass

production and widespread application of SiNPs would inevitably increase human exposure *via* occupational, environmental or even iatrogenic ways. Besides, SiNPs could enter into the natural environment through dust, construction, fuel combustion, etc., due to silicon is one of the most abundant minerals on Earth [4, 5]. Indeed, SiNPs was frequently used as the representative for atmospheric particulate matter (PM) study [6]. Nevertheless, there is still a lack of biosafety data related to SiNPs, and discrepancy exists in acquired toxicological evidence, probably owing to different exposure scenarios (e.g., *in vivo* vs *in vitro*, acute vs chronic) [7, 8].

Despite the most important route of exposure to SiNPs being inhalation, especially in occupational settings, cardiovascular system was a principal site of extra-pulmonary toxic effects of SiNPs. It is well-known that the inhaled NPs could pass through the air-blood barrier, owing to their small size. In support of this notion, as early as in 2002, Nemmar et al. reported the inhaled NPs can be detected in blood already after 1 minute [9]. Even the inhaled particles with the size up to 2.0 μm could be detected in extrapulmonary organs [10]. We previously detected a remarkable increase of silicon content in both serum and heart of SiNPs-treated rats *via* intratracheal instillation [11]. Research also found that nanoparticle translocation into atherosclerotic plaques in mouse aortic arch and human carotid artery after inhalation [12]. In despite of cardiovascular system as an important toxic site of NPs exposure, the current knowledge regarding the bio-toxic impact of NPs on the cardiovascular system was not fully clarified, and also the potential toxic mechanisms of NPs are still being questioned [13].

Epidemiological studies have demonstrated a closer correlation between atmospheric ultrafine particles (UFP) and cardiovascular diseases (CVDs) [14]. Owing to the similar physicochemical properties and biological actions between UFP and engineered NMs [15], the robust epidemiological investigations on UFP may lay foundation for the cardiovascular studies of NPs [16, 17]. So far, limited epidemiological or occupational evidence has documented the adverse cardiovascular effects caused by NPs exposures presently. Liao et al. found that the prevalence of arrhythmia and angina were significantly higher in NMs handling workers than in the controls, and cardiovascular markers (vascular cell adhesion molecule, intercellular adhesion molecule-1 and low frequency of heart rate variability) were significantly associated with handling SiNPs [18]. However, cardiovascular dysfunction was not found to be significantly associated with nanomaterials handling in their four-year panel study, probably attributing to selection bias and also indicating a more focus on long-term health effect in the future evaluation of cardiovascular toxicity of NPs.

Atherosclerosis is the major cause of CVDs, and its global burden is projected to rise substantially in the next few decades, particularly in developing low- and middle-income countries [19, 20]. However, whether SiNPs could cause the adverse effects on the formation and progression of atherosclerotic plaque is still poorly understood. Limited studies provided the vascular injury and dysfunction caused after SiNPs inhalation, probably associated with oxidative stress and inflammatory response [21]. In contrast, some studies found SiNPs had good biocompatibility as evidenced by no influence on cell viability or membrane integrity [22, 23]. Owing to controversial results and to the lack of sufficient data to clearly identify the pro-atherogenic effects of SiNPs, we firstly investigated the long-term influence of SiNPs on

the progression of atherosclerotic plaque by using ApoE-knockout ($ApoE^{-/-}$) mice fed a Western diet. $ApoE^{-/-}$ mice at the age of 1–2 months is commonly used as the animal model for spontaneous atherosclerosis [24]. To be noted, the ultrasound biomicroscopy, a useful tool for the non-invasive, dynamic characterization of blood vessels in animal models, was applied during the experiment. Consequently, we revealed the acceleratory effect of SiNPs on the development and progression of atherosclerosis in $ApoE^{-/-}$ mice, as evidenced by more severe hyperlipidemia, vascular stiffness, larger plaque area and lipid deposition after intratracheally instilled SiNPs. In agreed with the endoplasmic reticulum (ER) expansion and a higher expression of the ER stress marker (Bip and CHOP) in plaque, the related mechanism investigation by using the mouse macrophage cell line, RAW264.7 and an ER stress inhibitor, 4-PBA, revealed that the activation of ER stress mediated CD36 up-regulation to facilitate cholesterol influx and the formation macrophages-derived foam cells, which contributed to the plaque progression and ensuing CVDs. The current study may provide persuasive evidence for safety evaluation and risk management of SiNPs, and offered a new insight into the mechanisms underlying the adverse effects of SiNPs on cardiovascular system.

Result

Characterization of SiNPs

SiNPs were spherical in shape and uniform in size as manifested by the SEM and TEM images (Fig. 2A, B). The particle diameter was normally distributed, with a mean value of 59.98 nm as measured by Image J software (Fig. 2C). Hydrodynamic size and Zeta potential were commonly detected as indicators of particle dispersion and stability. As a result, the hydrodynamic size and Zeta potential of SiNPs in deionized water were relatively stable at different time points (0–24 hours), which were approximately 95 nm and − 35 mV, respectively (Fig. 2D and Table 1). In addition, SiNPs were sterilized and endotoxin-negative, with purity more than 99.9%.

Table 1. The hydrodynamic size and zeta potential of SiNPs in deionized water at different timepoints.

Time (h)	Diameter (nm)	Zeta potential (mV)
0	96.23 ± 3.76	-36.40 ± 3.13
3	102.15 ± 9.08	-36.46 ± 1.25
6	90.83 ± 3.07	-40.30 ± 2.48
12	89.60 ± 3.65	-34.63 ± 1.15
24	95.48 ± 5.31	-33.86 ± 1.53

Note: Data are expressed as mean ± SD, n=3.

Vascular stiffing promoted by SiNPs

During the 20-week Western diet feeding and SiNPs treatment, a UBM system was applied to monitor the vascular function and plaque formation. Finally, as depicted in Fig. 3A, an obvious plaque in the LCCA was observed, and the plaque area was increased slightly after SiNPs treatment. Moreover, IMT and PWV in each group were gradually increased, while the area/diameter percentage spread (changes in displacement of blood vessels during a cardiac cycle) and global radial strain were declined at different timepoint (Fig. 3B), which is consistent with the process of atherosclerosis. To be noted, PWV value of LCCA was significantly greater in SiNPs group (6.0 mg/kg·bw) when compared to control group, indicating vascular stiffening aggravated by SiNPs exposure.

Atherosclerotic plaque progression promoted by SiNPs

As depicted in Fig. 4A, mice in each group had significant plaque formation in the aorta, and no significant difference was observed on the number and distribution of plaque in the whole aorta (Fig. 4B and C). Further, H&E, Oil-Red O, Masson staining of aortic root sections were used to quantify the plaque burden (Fig. 4D). As shown in Fig. 5E and F, the lesion area and maximum plaque thickness were remarkably increased in SiNPs group (6.0 mg/kg·bw) than in control group ($p < 0.05$). Oil-Red O staining revealed a slight increase trend of lipid content after SiNPs exposure, but no statistical significance, which was probably attributed to the higher plaque area in SiNPs-treated mice (Fig. 4G). Collagen content was markedly increased in mice exposed to SiNPs (Fig. 4H). The negative staining of alizarin red indicated no calcification occurred inside the plaque (Fig. 4D). In addition, the ultrastructure observation by TEM provided evidence for the performance of advanced plaque lesions in $ApoE^{-/-}$ mice, which were characterized with endothelial injury, macrophage adhesion to the vascular endothelial cell, foam cell, smooth muscle cell migration, cholesterol crystal, and even necrotic substances (Fig. 5). Of note, ER expansion was clearly seen in macrophage within plaque.

Dyslipidemia promoted by SiNPs

Compared with the control group, mice in SiNPs groups had markedly elevated TG and LDL-C levels and calculated AI, and declined HDL-C/LDL-C ratio, especially at the dose of 6.0 mg/kg·bw group ($p < 0.05$), in despite of no significant difference in TC and HDL-C levels (Fig. 6A-F). In addition, there was a positive correlation between serum LDL-C content and plaque area in aortic root, which suggested that mice with higher serum LDL-C content had a larger plaque load (Fig. 6G).

ER stress of macrophage triggered by SiNPs in plaque

As shown in Fig. 7, the up-regulated expressions of CD68, Bip and Chop in the plaque of SiNPs-treated mice were detected, mainly on the luminal side of the lesion, indicating a greater macrophage infiltration and ER stress induced by SiNPs. Simultaneously, the positive expression positions of CD68, Bip and CHOP were almost completely overlapping, reflecting the activation of ER stress mainly in macrophage or macrophage-derived foam cells.

Particle uptake and ER stress triggered by SiNPs in macrophages

As depicted in Fig. 8A, the presence of large quantity of protrusions and particle aggregates could be clearly observed on the SiNPs-treated cell surface. Meanwhile, the intracellular particles were deposited in cytoplasma of macrophage, mostly in autophagic vacuoles, according to the TEM images (Fig. 8B). Further, the intracellular particles were verified to be internalized SiNPs as evidenced by the determination of silicon and oxygen elements using energy spectrum scanning (Fig. 8C). In addition, the TEM images also showed a significant expansion and degranulation of ER in SiNPs-treated macrophage (Fig. 8D). In consistent with the TEM images, the protein expressions of Bip and CHOP were significantly up-regulated after SiNPs exposure (Fig. 8E). All these results suggested that SiNPs could be up-taken by macrophage, and subsequently triggered ER stress.

ER stress enhanced lipid accumulation and macrophage-derived foam cell formation by SiNPs

Macrophage-derived foam cell formation was a hallmark event during the progression of atherosclerotic lesion. As shown in Fig. 9A, Oil-Red O staining displayed that SiNPs aggravated the intracellular content of lipid droplets under oxLDL cotreatment, however, 4-PBA pretreatment alleviated this phenomenon. Similarly, as illuminated in Fig. 9B, SiNPs treatment caused an increase in the content of intracellular TC, either with or without oxLDL cotreatment, which also can be alleviated by 4-PBA. Therefore, results validated that SiNPs promoted lipid accumulation through ER stress-mediated way, consequently contributing to the foam cell formation and plaque progression.

ER stress-mediated CD36 upregulation involved in lipid accumulation in macrophage by SiNPs

The intracellular lipid homeostasis in macrophage was precisely regulated by lipid influx and efflux. Thus, we further detected the expressions of factors controlling the cholesterol uptake (CD36 and SRA1) and its efflux (ABCA1, ABCG1, and SRB1) in macrophage. Real-time PCR results showed that SiNPs exposure caused the up-regulated mRNA expressions of CD36 and SRA1, while down-regulated mRNA expressions in ABCA1, ABCG1, and SRB1. In addition, SiNPs had no influence on the mRNA level of ACAT1, a critical regulator to re-esterify excessive free cholesterol to cholesterol ester to store in lipid droplets [25]. Further, 4-PBA was applied to validate the role of ER stress in the regulation of lipid homeostasis. Results validated that the up-regulation of CD36 was positively regulated by ER stress, owing to a significant decline of CD36 in 4-PBA plus SiNPs group when compared to the SiNPs group (Fig. 10A). Moreover, such phenomenon was also verified at the protein level of CD36 (Fig. 10B), indicating that the induction of ER stress by SiNPs could simulate CD36 expression, leading to more lipid uptake and accumulation in macrophage. In addition, the expression of CD36 in the lesions of SiNPs-treated mice was also elevated according to the immunohistochemical analysis (Fig. 10C).

Discussion

Atherosclerotic related cardiovascular disease is the leading cause of mortality worldwide. So far, there is still no conclusive information on the pro-atherogenic potential of SiNPs. To the best of our knowledge, this is the first *in vivo* study to confirm SiNPs exposure could indeed accelerate the progression of atherosclerosis. We firstly administered Western diet-fed ApoE$^{-/-}$ mice with SiNPs or saline through intratracheal instillation for 12 weeks, and ultrasound biomicroscopy (UBM) was applied to monitor the development and progression of atherosclerosis. Epidemiological studies have provided a close correlation between $PM_{2.5}$ and carotid intima-media thickness (CIMT), a most frequently used indicator of subclinical atherosclerosis [26]. However, only few studies reported the vascular effects of NPs through Doppler ultrasound trace. Here, ultrasound technique was applied, and repeated measurement data was acquired, which would be more convincing. As a result, the data indicated the atherosclerosis model was well established, and SiNPs exposure reduced arterial elasticity, aggravated the arterial stiffness, which is a feature of atherosclerotic plaque progression [27]. Arterial stiffness was positively correlated with reactive oxygen species (ROS) and the followed oxidative stress [28], a major attributor of the adverse effects caused by SiNPs, and inversely with arterial NO bioavailability. A declined NO bioavailability was detected as a decrease in endothelium-dependent vasodilatation [29]. Indeed, a disturbed oxidation-reduction status was triggered after intratreacheally instilled SiNPs [21], as well as NO/NOS disorder.

On the basis of a clearly observed plaque and an increased PWV value in SiNPs-treated mice, the experiment was terminated, and atherosclerotic burden was assessed by en-face staining of the whole aorta and histological examination of the aortic root. Consistent with the UBM monitoring, plaque was formed in aorta, and the plaque area and lipid-rich core area in plaque were increased after SiNPs administration. Plaques with lipid-rich cores are suspected to be vulnerable, increasing the risk of sudden plaque rupture and thrombotic complications. Previous studies have found the induction of systemic inflammation by SiNPs [30], probably contributing to the form of vulnerable plaques [31]. In addition, according to the American Heart Association's definition of human atherosclerotic stages [32, 33], the plaque at the termination of experiment was progressed into advanced lesion with stage IV, characterized with the large plaque burden and foam cells, migrating smooth muscle cells, cholesterol crystals, and necrotic substances inside the plaque. Previously, SiNPs was confirmed to induce endothelial injury [34, 35, 36, 37] and promote the recruitment of monocytes to injured endothelial cells [38], and foam cell formation at the early stage of atherosclerosis [39]. Moreover, a discontinued or fragmented intimal surface was induced by repeated pulmonary exposure of SiNPs, accompanied with endothelial apoptosis [21]. In addition, the ability to induce thrombosis formation may also attribute to the pro-atherogenic potential of SiNPs [40]. However, the underlying mechanisms by which SiNPs influenced atherogenesis still remains largely unknown.

Lipid is one of the most important stimuli initiating atherogenesis. Plasma lipoproteins are involved in foam cell formation and inflammatory regulation within plaques [41, 42, 43]. The abnormal plasma lipoprotein level is usually considered as the feature of atherosclerosis. To date, few studies have pointed out the induction of dyslipidemia by airborne UFP [44]. Repeated intravenous administration of SiNPs

was reported to disturb hepatic lipid metabolism and trigger hyperlipidemia in mice [45]. Similarly, dys- or hyper-lipidemia was induced after a long-term exposure of ZnO NPs *via* intratracheally instillation in rat, or of TiO_2 NPs in ICR or $ApoE^{-/-}$ mice, ultimately contributing to the initiation and progression of atherosclerosis [46, 47, 48, 49]. In particular, a cross-sectional study also found that occupational exposure to TiO_2 NPs affected lipid metabolism, as evidenced by a higher level of serum LDL when compared to the normal physiologic range for LDL in adults in China [50]. In agreement with these findings, we revealed the sub-chronic SiNPs treatment *via* intratracheal instillation also aggravated the hyperlipidemia of $ApoE^{-/-}$ mice, characterized with the increased serum levels of TG and LDL-C. To be noted, the increase in serum LDL-C content was positively correlated with the plaque area in aortic root. Coincidently, population studies have shown a highly consistent, positive correlation between blood LDL-C level and atherosclerotic CVD risk in humans [51]. Besides, hypertriglyceridemia is causally associated with increased atherosclerosis risk [42]. Intriguingly, either the repeated exposure to single-wall carbon nanotube (SWCNT) or long-term (over 5 months) exposure of nano-Ni was reported to exacerbate plaque development in $ApoE^{-/-}$ mice, but no alteration of lipid profile [49, 52]. It might explain other mechanisms also contributing to atherogenesis, such as systemic oxidative stress, inflammation [53].

Endoplasmic reticulum (ER) stress, also known as unfold protein response (UPR), plays a crucial role in the pathogenesis of a series of cardiovascular disorders, including atherosclerosis, ischemia. ER is a major site for protein folding and calcium reservoir. Numerous studies suggested ER as a potential target for NPs [34, 54, 55, 56, 57, 58]. The accumulation of misfolded or unfolded proteins led to ER stress, which was recently proposed as the mechanism responsible for NPs-induced toxicity [59]. ER stress could occur at all stages of atherogenesis [60]. Moreover, studies by using human plaque samples and animal models showed an increased ER stress in plaques with faster plaque progression [61]. The induction of ER-associated UPR events by NPs was pointed out either in vitro or in vivo [34, 62]. In particular, other than oxidative stress, ER stress was reported to mediate the SiNPs-caused vascular injury in rats [21], and modulate ROS formation in vascular endothelial cells, which could be explained by the increased ROS as an integral component of UPR signaling [63]. At the present study, aggravated ER stress in macrophage within plaque was clearly seen, as evidenced by ER expansion and remarkably elevated Bip and CHOP levels. But how ER stress participates and its regulatory molecular mechanism among the pro-atherogenesis effect of SiNPs was still unclearly illuminated.

Macrophage-derived foam cell is the crucial determinant of the initiation and progression of atherosclerosis lesion [64], contributing to plaque instability and rupture [65]. In agreement with previous studies [39], ER stress was significantly induced after SiNPs exposure, as evidenced by the expansion and degranulation of ER, as well as greatly up-regulated Bip and CHOP expressions. More importantly, ER stress inhibition largely alleviated the lipid accumulation induced by SiNPs in macrophage as assessed by the Oil-Red O staining and intracellular cholesterol measurement. It is worth noting that some ER stress genes are involved in lipid metabolism, which fuel atherogenesis. For instance, CHOP is crucial for lipid synthesis, and its expression would result in lipid accumulation [66]. The cellular lipid homeostasis was highly, precisely regulated by lipid influx and efflux. Upon oxLDL and SiNPs co-exposure, remarkably

dysregulated expressions of lipid influx/efflux genes were detected in macrophage [39], probably mediated by ER stress signaling. Further, Long et al. revealed the lipid accumulation in macrophages was attributed to the modulation of ER stress leading to the upregulation of scavenger receptors, including CD36 and SRA1 [67]. Apart from CD36, ER stress was also reported to correlate with reduced ABCA1 level in macrophage, a key regulator for lipid efflux. But that was not the case in SiNPs-induced lipid accumulation. However, our data confirmed only CD36 was dependent on ER stress induced by SiNPs, leading to lipid accumulation and foam cell formation, ultimately contributing to atherosclerosis. CD36 is a membrane glycoprotein that belongs to the class B scavenger receptor family, and is known to be involved in lipid metabolism as well as atherosclerosis development. Indeed, a series of studies have proven ER stress modulated lipid influx *via* CD36 [70, 71, 72]. Lipid could be trafficked by CD36 to ER, and meanwhile, the accumulation of toxic lipids in macrophages would result in a prolonged ER stress. However, the detailed molecular mechanisms by which ER stress regulate CD36 need to address in future studies. Of note, the enhanced intracellular cholesterol content and the modulation of cholesterol influx/efflux genes could be directly induced by SiNPs even without external lipid supply, indicating the excessive lipids are not indispensable for SiNPs to promote foam cell formation.

By the way, how do the applied doses relate to a real-life exposure? The air concentrations of amorphous SiNPs ranged 400–22200 particles/cm^3 [73]. The number of NPs in ambient air ranged from 2×10^4 to 2×10^5/cm^3, with mass concentrations of > 50 μg/m^3 near major highways [74]. Here, the actual lung exposure dose of SiNPs (1.5, 3.0 or 6.0 mg/kg·bw) was about 40, 80, 160 μg/mouse/week (based on mice weighting 26–29 μg during SiNPs treatment), respectively. According to a previous study [48], the inhalation dose of a mouse is about 5 μg after a one-week exposure at the daily concentration of 50 μg/m^3 near major highways (consuming the inhalation rate for mice is 0.052 m^3/day, and the mice pulmonary deposition fraction for 60 nm particles of 0.25) [75]. In this concentration, the applied dose (1.5, 3.0 or 6.0 mg/kg·bw) in this study was correspondingly 8, 16, or 32 times to the airborne exposure level of SiNPs. Hence, this study is featured by the used exposure conditions relevant to human exposure scenarios.

Conclusions

In summary, this is the first study to directly address the acceleratory effect of SiNPs in atherosclerotic plaque progression by using $ApoE^{-/-}$ mice. And also, it is novel in the utilization of ultrasonic technique to non-invasive, dynamic assess the vascular function and plaque formation. Consequently, the current study demonstrated an increased plaque size, macrophage infiltration and lipid deposition in the aortic root after long-term SiNPs exposure *via* intratracheal instillation, accompanied by the aggravated hyperlipidemia, artery stiffness and ER stress in plaque. Moreover, a comprehensive molecular mechanism related to the promotion of atherosclerotic progression by SiNPs was provided. That was, ER stress-mediated up-regulated CD36 expression was validated to be a major contributor of SiNPs to promote foam cell formation and ultimate plaque progression. Hence, SiNPs exposure was proposed as a

risk factor for atherosclerotic CVD, and more efforts should be made for a safer application of nanoproducts.

Methods

Nanoparticles preparation and characterization

The amorphous SiNPs used in the experiments were prepared by the Stöber method as previously described [36]. The shape and size of the nanoparticles were observed by scanning electron microscopy (SEM; Hitachi S-4800, Japan) and transmission electron microscopy (TEM; JEM2100, Japan). Based on the TEM results, the particle size distribution was analyzed through Image J software. The hydrodynamic size and Zeta potential of SiNPs in deionized water were measured by Zetasizer (Malvern Nano-ZS90, UK). Moreover, an inductively coupled plasma atomic emission spectrometry (ICP-AES; Agilent 720, USA) was used for the purity detection of the synthesized SiNPs, and a gel-clot limulus amebocyte lysate (LAL) assay kit (Bokang, Zhanjiang, China) for endotoxin measurement. In addition, the stock suspension of SiNPs were firstly dispersed by a sonicator (160 W, 20 kHz, 5 min; Bioruptor UCD-200, Belgium), and then diluted by the corresponding exposure media, 0.9% saline (*in vivo* test) or DMEM (*in vitro* test).

Animal studies

Male ApoE$^{-/-}$ mice (age, four-week; weight, 18–22 g), a well-established animal model for atherosclerosis, were obtained from the Experimental Animal Center of Capital Medical University (Beijing, China) to assess the long-term effect of SiNPs in the development of atherosclerosis. All mice were housed in sterilized filter-topped cages with free access to food and water, and maintained in a specific pathogen-free facility with a constant humidity (50 ± 5%), temperature (24 ± 1 °C) at 12/12-h light/dark cycle. After one week of acclimation, all the mice were supplied with a Western diet (21% fat, 0.15% cholesterol, 34% sucrose) for 20 weeks. Four-week later, the mice were randomly divided into four groups (12 mice per group), which were control group and three SiNPs groups at a dose of 1.5, 3.0, or 6.0 mg/kg·bw, respectively. The applied dose of SiNPs was in reference to an inhalation study in mice [76], in which the doses of SiNPs were evaluated based on the real workplace exposure scenarios. It was reported the occupational exposure level of SiNPs ranged from 1.0–27.6 mg/m^3 [77]. In considering the lack of a recommended exposure limit for amorphous SiNPs, the permissible concentration-time weighted average (PC-TWA) of amorphous silica dioxide (SiO_2), 6 mg/m^3 was used. Therefore, a worker (60 kg) exposed to a concentration of 6 mg/m^3 SiNPs for 8 h (1 workday) without proper protection will result in an approximate pulmonary dose of 0.44 mg/kg·bw (assuming human under a light exercise condition in workplace with breathing frequency 20 breaths/min, 1024 mL/breath, and pulmonary deposition fraction for 60 nm particles of 0.45 in human) [75, 78]. According to the equivalent conversion coefficient of the dose per kilogram of body weight in experiment animals and human [79], the dosage is equivalent to 5.45 mg/kg·bw in mice. Thus, we set the highest dose as 6.0 mg/kg·bw.

Mice in SiNPs groups were administered SiNPs suspension through intratracheally instillation, once in every 7 days and 12 times in total, whereas the control mice were instilled with 0.9% saline instead. The volume of intratracheal instillation was controlled to be 50 ± 5 μl. Furthermore, the ultrasound biomicroscopy (UBM) of three mice per group was performed at the 4th, 10th, 16th, and 20th week. The experimental design is shown in the Fig. 1. In addition, the body weight and food intake of mice were monitored and weighed weekly (see details in the supplementary Fig. S1). At the termination of the experiment, mice were fasted overnight, blood and aortas were harvested. Serum was extracted from the blood and stored at -80 °C until analyzed. All the animal experimentation was performed following the National Guidelines for Animal Care and Use, and approved by the Committee of Laboratory Animal Care and Use in Capital Medical University (Ethical number, AEEI-2018-002).

Ultrasound biomicroscopy

An ultra-high resolution color doppler ultrasound system (Vevo 2100, FUJIFILM Visualsonics, USA) equipped with MS 400/550D mechanical transducers was used, and the ultrasound imaging parameters of the left common carotid artery (LCCA) were measured. During the experiment, mice were anaesthetized with isoflurane gas resulting in a heart rate of approximately 500 beats/min, and the hair from the anterior chest wall was carefully shaved, and warm ultrasound transmission gel was liberally applied to ensure optimal image quality. The intima-media thickness (IMT) and pulse wave velocity (PWV) were obtained using VEVO LAB software. The EKV two-dimensional dynamic image was analyzed by VEVO VASC software, and indicators representing vascular compliance (diameter/area percentage spread and global radial strain) were obtained. On the basis of a previous description [80], IMT is measured with the vascular lumen–intimal interface selected as the internal measurement site and the media–adventitial interface as the external limit. PWV was calculated by the following formula: Length of LCCA/Time of blood flowing through the LCCA. All measurements were repeated three times. All the images were analyzed by another operator blinded to the identities of the animals.

Lipid profiles analysis

The contents of total cholesterol (TC), total triglyceride (TG), high density lipoprotein cholesterol (HDL-C), and low-density lipoprotein cholesterol (LDL-C) in mice serum were measured by an automatic biochemical analyzer. The ratio of HDL-C/LDL-C and atherogenic index (AI) were calculated. AI was defined according to the formula: AI = (TC - HDL-C)/HDL-C.

Histopathological examination

For lesions throughout the aorta, the whole aortas of three mice per group were separated, cut longitudinally after removing excess adipose tissue, and stained with Oil-Red O staining (Solarbio, Beijing, China) for 10 minutes. Afterwards, the stained aortas were placed in 75% alcohol until the artery wall without lesions was cleaned. Images were captured and analyzed by Image J software. Furthermore, for the lesion at the aortic root, the entire aortic root was immersed in 4% paraformaldehyde for 24 hours, embedded into paraffin or optimal cutting temperature (OCT) for histological examination. The cross-

sections of the aortic root were stained with hematoxylin and eosin (H&E), Oil-Red O, Masson and Alizarin Red for the quantification of plaque area, lipid and collagen content, and aortic calcification. It is worth noting that the regional error in lesion size was avoided by acquiring of the sequential cross-sections throughout the entire aortic root as previously described [81]. Ultimately, the largest lesion area was selected for the comparative analysis of plaque (Supplementary material Fig. S2). All slides were scanned with Pannoramic SCAN system (3DHISTECH, Hungary), and measured with CaseViewer software (3DHISTECH, Hungary) or by Image J software. The quantification of each morphological parameter was performed by one investigator blinded for the treatment. The quantification of each morphological parameter was performed by one investigator blinded for the treatment, and reviewed by certified veterinary pathologists.

Immunohistochemical staining

Immunohistochemistry was performed in the paraffin-embedded artery root to determine the expressions of CD68 (a macrophage marker), CD36 (a principal contributor to cholesterol uptake), Bip and CHOP (biomarkers for endoplasmic reticulum stress) *in situ*. Briefly, the dehydrated paraffin sections were immersed in 1 mM EDTA (pH = 9) for antigen retrieval, and incubated with 3% hydrogen peroxide to abolish endogenous peroxidase. The sections were incubated with the primary antibody for CD68 (ab125212, Abcam, UK), CD36 (18836, Proteintech, USA), Bip (#3177, CST, USA), or CHOP (15204, Proteintech, USA) overnight at 4 °C, and then incubated with the corresponding secondary antibody and stained with 3,3’-diaminobenzidine (DAB). These primary antibodies were diluted with 5% BSA solution at a ratio of 1: 200. Moreover, the nucleus was stained with hematoxylin. Finally, the percentage of positive-staining area in the whole plaque of aortic root was analyzed using the Image J software. All analyses were performed by one investigator blinded for the treatment.

TEM observation of lesions

The ultrastructure of lesion was observed by using TEM (JEM2100; JEOL, Japan). In brief, the first branch of aorta was fixed by 2.5% glutaraldehyde overnight, rinsed with 0.1 M phosphate buffer, and postfixed with osmic acid for 2 hours. After being dehydrated in ethanol with concentration gradients and acetone, the sample was embedded in epoxy resin. Ultimately, the ultrathin sections (50 nm) were obtained and imaged under TEM.

Cell culture and treatment

Mouse macrophage cell line, RAW264.7 cells were cultured in DMEM (ThermoFisher, USA) with 10% fetal bovine serum (FBS; ThermoFisher, USA) at 37 °C in a 5% CO2 incubator. SiNPs were diluted by DMEM to appropriate concentrations, and an ER stress inhibitor, 4-phenylbutyric acid (4-PBA; Selleck, USA) was applied (3 mM, 6 hours). The dosage of SiNPs was set according to the cell viability analysis by using MTT assay. Since a significant acute toxicity (24 hours) was seen in SiNPs-treated group at a concentration of 50 μg/ml, while simultaneously with cell viability > 70%, the exposure mode of SiNPs (50 μg/ml, 24 hours) was used in the subsequent *in vitro* experiments. Similarly, the application of 4-PBA was set up through MTT assay and also verified as evidenced by an efficient inhibition on the up-

regulated expressions of Bip and Chop induced by SiNPs. See details in the supplementary Fig. S3. After SiNPs with or without 4-PBA treatment, cells were harvested for the following measurement.

Cellular morphology observation and particle internalization analysis

After 50 μg/ml SiNPs treatment for 24 hours, the cellular morphology and alterations of cellular ultrastructure were observed by SEM (S-4800, Hitachi, Japan), and TEM (JEM2100, JEOL, Japan). Based on the TEM image, the particle uptake and internalization were verified by energy dispersive spectrometry (EDS; Bruker-XFlash6/60, Germany).

Intracellular lipid measurement

Intracellular lipid droplets were determined by Oil-Red O staining as previously described [39]. In brief, cells were fixed with 4% paraformaldehyde, and stained with Oil-Red O working solution for 30 minutes after assimilation of 60% isopropanol. The excess dye was washed away with 60% isopropanol and the cells were observed under an Olympus IX81 microscope (Tokyo, Japan). Also, the intracellular content of total cholesterol (TC) was measured by a total cholesterol assay kit (Applygen, Beijing, China) according to the manufacturer's protocol. Ultimately, the intracellular TC content was calibrated using protein mass.

Quantitative real-time RT-PCR

The total cellular RNA was extracted by using a RNAsimple Total RNA kit (Tiangen, Beijing, China), and reversely transcribed to cDNA using a PrimeScript™ RT reagent kit (TaKaRa, Japan). The quantitative PCR was performed by using the SYBR Premix Ex TaqTM II (Takara, Japan) in a real-time PCR machine (Bio-Rad, USA). The relative expression in mRNA levels of lipid transport (CD36, SRA1, ABCA1, ABCG1 and SRBI) and esterification (ACAT1), and also endoplasmic reticulum (ER) stress indicators (Bip and CHOP) were quantified. Each experiment was conducted in triplicate with β-actin as the internal standard. Primers used for quantitative PCR analysis were listed in the supplementary file (Table S1).

Western Blot assay

The whole cellular protein was extracted by a Protein Rapid Extraction kit (KeyGEN, China), and quantified by BCA protein assay (Dingguo, China). After denaturation, protein lysate was separated with SDS-PAGE, and transferred to a nitrocellulose membrane (Pall, Germany). The membrane was blocked with Tris-buffered saline (TBS) solution containing 5% skim milk powder for 1 hour at room temperature. After wash three times with TBST (TBS with 0.05% Tween-20), membrane was incubated with the primary antibody diluted by TBST solution (1 : 1000), including Bip (#3177, CST, USA), CHOP (#2895, CST, USA), CD36 (ab64014, Abcam, UK), GADPH (#5174, CST, USA) and β-actin (66009, Proteintech, USA) overnight. After three-time wash with TBST, membrane was incubated with the corresponding fluorescent secondary antibody (LI-COR, Gene Company Limited, Hong Kong) for 1 hour at room temperature, and ultimately detected using Odyssey® CLx imaging system (Gene Company Limited, Hong Kong). At least three independent experiments were performed. The relative expression level of protein was analyzed by Image

Studio™ quantification software (Gene Company Limited, Hong Kong) with β-actin or GAPDH as internal control, and normalized to the control group.

Statistical analysis

Data were expressed as mean ± standard deviation. Beside the ultrasound data by repeated measures analysis of variance (ANOVA) and CD36 expression in plaque by t-test of independent samples, the significant analysis for the *in vivo* study was determined by one-way ANOVA. Significance for the *in vitro* experiment was analyzed by t-test of independent samples, except for the statistical analysis of Bip or CHOP expression in RAW264.7 cells by one-way ANOVA. A two-tailed Person correlation test was applied to determine the correlation between the lesion areas in aortic root and serum lipid levels. All data were analyzed by SPSS 20.0 software, and p value < 0.05 indicates statistical significance.

Declarations

Availability of data and material

The datasets used and/or analyzed during the current study are available from the corresponding author on reasonable request.

Ethical Approval and Consent to participate

All the animal experimentation was performed following the National Guidelines for Animal Care and Use, and approved by the Committee of Laboratory Animal Care and Use in Capital Medical University (Ethical number, AEEI-2018-002).

Consent for publication

Not applicable.

Competing interests

The authors declare that they have no competing interests.

Funding

This work has been financially supported by the National Natural Science Foundation of China (81872648, 81573176), Scientific Research Common Program of Beijing Municipal Commission of Education (KM201810025007), Beijing Education Committee Program for Cultivation of Young Top-notch

Personnel in Beijing Municipality (CIT&TCD201804090), and General Program of Beijing Natural Science Foundation (7162021).

Authors' contributions

The authors GC and LY are responsible for the study design. MR, QY, ZX, LX and SX participate the experimental implementation and data analysis. MR, GC and LY are responsible for writing and revising of the manuscript. GC, LY, NP, CR and SZ have contributions on reagents/materials/analysis tools. All the authors read and approved the final manuscript.

Acknowledgements

We thank to Qing Xu and Jingjing Wang from the Experimental Center of Capital Medical University for their technical support during the animal experiment.

References

1. Organization WH. WHO Guidelines on Protecting Workers from Potential Risks of Manufactured Nanomaterials.; 2017.
2. Geary SM, Morris AS, Salem AK. Assessing the effect of engineered nanomaterials on the environment and human health. J ALLERGY CLIN IMMUN. 2016;138(2):405–8.
3. Winkler HC, Suter M, Naegeli H. Critical review of the safety assessment of nano-structured silica additives in food. *J NANOBIOTECHNOL* 2016, 14(1).
4. Matassoni L. Saharan dust contribution to PM10,PM2.5 and PM1 in urban and suburban areas of Rome: a comparison between single-particle SEM-EDS analysis and whole-sample PIXE analysis. *Journal of Environmental Monitoring* 2011(13):732–742.
5. Moreno T, Reche C, Rivas I, Cruz Minguillón M, Martins V, Vargas C, Buonanno G, Parga J, Pandolfi M, Brines M, et al. Urban air quality comparison for bus, tram, subway and pedestrian commutes in Barcelona. ENVIRON RES. 2015;142:495–510.
6. Lu C, Li L, Zhou W, Zhao J, Wang Y, Peng S. Silica nanoparticles and lead acetate co-exposure triggered synergistic cytotoxicity in A549 cells through potentiation of mitochondria-dependent apoptosis induction. ENVIRON TOXICOL PHAR. 2017;52:114–20.
7. Vance ME, Kuiken T, Vejerano EP, McGinnis SP, Hochella JMF, Rejeski D, Hull MS. Nanotechnology in the real world: Redeveloping the nanomaterial consumer products inventory. BEILSTEIN J NANOTECH. 2015;6(1):1769–80.
8. Murugadoss S, Lison D, Godderis L, Van Den Brule S, Mast J, Brassinne F, Sebaihi N, Hoet PH. Toxicology of silica nanoparticles: an update. ARCH TOXICOL. 2017;91(9):2967–3010.

9. Nemmar A, Hoet DP,PHM, Vanquickenborne PB, Dinsdale MD, Thomeer PM, Hoylaerts MMF, Vanbilloen PH, Mortelmans PL, Nemery MP,B MP. Brief Rapid Communications Passage of Inhaled Particles Into the Blood Circulation in Humans. *CIRCULATION* 2002, 4(105):411–414.
10. Li D, Li Y, Li G, Zhang Y, Li J, Chen H. Fluorescent reconstitution on deposition of PM2.5 in lung and extrapulmonary organs. *Proceedings of the National Academy of Sciences* 2019, 116(7):2488–2493.
11. Du Z, Zhao D, Jing L, Cui G, Jin M, Li Y, Liu X, Liu Y, Du H, Guo C, et al. Cardiovascular Toxicity of Different Sizes Amorphous Silica Nanoparticles in Rats After Intratracheal Instillation. CARDIOVASC TOXICOL. 2013;13(3):194–207.
12. Miller MR, Raftis JB, Langrish JP, McLean SG, Samutrtai P, Connell SP, Wilson S, Vesey AT, Fokkens PHB, Boere AJF, et al. Inhaled Nanoparticles Accumulate at Sites of Vascular Disease. ACS NANO. 2017;11(5):4542–52.
13. Yu X, Hong F, Zhang YQ. Bio-effect of nanoparticles in the cardiovascular system. J BIOMED MATER RES A. 2016;104(11):2881–97.
14. Downward GS, van Nunen EJHM, Kerckhoffs J, Vineis P, Brunekreef B, Boer JMA, Messier KP, Roy A, Verschuren WMM, van der Schouw YT, et al. Long-Term Exposure to Ultrafine Particles and Incidence of Cardiovascular and Cerebrovascular Disease in a Prospective Study of a Dutch Cohort. ENVIRON HEALTH PERSP. 2018;126(12):127007.
15. Stone V, Miller MR, Clift MJD, Elder A, Mills NL, Møller P, Schins RPF, Vogel U, Kreyling WG, Alstrup Jensen K, et al. Nanomaterials Versus Ambient Ultrafine Particles: An Opportunity to Exchange Toxicology Knowledge. ENVIRON HEALTH PERSP. 2017;125(10):106002.
16. Ostro B, Hu J, Goldberg D, Reynolds P, Hertz A, Bernstein L, Kleeman MJ. Associations of Mortality with Long-Term Exposures to Fine and Ultrafine Particles, Species and Sources: Results from the California Teachers Study Cohort. ENVIRON HEALTH PERSP. 2015;123(6):549–56.
17. Gwinn MR, Vallyathan V. Nanoparticles: health effects–pros and cons. Environ Health Perspect. 2006;114(12):1818–25.
18. Liao HY, Chung YT, Lai CH, Lin MH, Liou SH. Sneezing and allergic dermatitis were increased in engineered nanomaterial handling workers. IND HEALTH. 2014;52(3):199–215.
19. Barquera S, Pedroza-Tobías A, Medina C, Hernández-Barrera L, Bibbins-Domingo K, Lozano R, Moran AE. Global Overview of the Epidemiology of Atherosclerotic Cardiovascular Disease. ARCH MED RES. 2015;46(5):328–38.
20. Hay SI, Abajobir AA, Abate KH, Abbafati C, Abbas KM, Abd-Allah F, Abdulkader RS, Abdulle AM, Abebo TA, Abera SF, et al. Global, regional, and national disability-adjusted life-years (DALYs) for 333 diseases and injuries and healthy life expectancy (HALE) for 195 countries and territories, 1990–2016: a systematic analysis for the Global Burden of Disease Study 2016. The Lancet. 2017;390(10100):1260–344.
21. Li Y, Ma R, Liu X, Qi Y, Abulikemu A, Zhao X, Duan H, Zhou X, Guo C, Sun Z. Endoplasmic reticulum stress-dependent oxidative stress mediated vascular injury induced by silica nanoparticles in vivo and in vitro. *NanoImpact* 2019, 14:100169.

22. Uboldi C, Giudetti G, Broggi F, Gilliland D, Ponti J, Rossi F. Amorphous silica nanoparticles do not induce cytotoxicity, cell transformation or genotoxicity in Balb/3T3 mouse fibroblasts. Mutation Research/Genetic Toxicology Environmental Mutagenesis. 2012;745(1–2):11–20.
23. Malvindi MA, Brunetti V, Vecchio G, Galeone A, Cingolani R, Pompa PP. SiO2 nanoparticles biocompatibility and their potential for gene delivery and silencing. NANOSCALE. 2012;4(2):486–95.
24. Zhang SHRRPJ. Spontaneous hypercholesterolemia and arterial lesions in mice lacking apolipoprotein E. SCIENCE. 1992;258:468–71.
25. Fernandez-Ruiz I, Puchalska P, Narasimhulu CA, Sengupta B, Parthasarathy S. Differential lipid metabolism in monocytes and macrophages: influence of cholesterol loading. J LIPID RES. 2016;57(4):574–86.
26. Aguilera I, Dratva J, Caviezel S, Burdet L, de Groot E, Ducret-Stich RE, Eeftens M, Keidel D, Meier R, Perez L, et al. Particulate Matter and Subclinical Atherosclerosis: Associations between Different Particle Sizes and Sources with Carotid Intima-Media Thickness in the SAPALDIA Study. ENVIRON HEALTH PERSP. 2016;124(11):1700–6.
27. Di Lascio N, Kusmic C, Stea F, Faita F. Ultrasound-based Pulse Wave Velocity Evaluation in Mice. *Journal of Visualized Experiments* 2017(120).
28. Mozos I, Luca CT. Crosstalk between Oxidative and Nitrosative Stress and Arterial Stiffness. CURR VASC PHARMACOL. 2017;15(5):446–56.
29. Xiao J. Exercise for Cardiovascular and Treatment.; 2017.
30. Nemmar A, Beegam S, Yuvaraju P, Yasin J, Attoub S, Ali B, Albarwani S. Amorphous silica nanoparticles impair vascular homeostasis and induce systemic inflammation. *INT J NANOMED* 2014:2779.
31. Maria Drakopoulou KTAM. Vulnerable Plaque and Inflammation: Potential Clinical Strategies. CURR PHARM DESIGN. 2011;37(17):4190.
32. Herbert C. Stary MCAB. A Definition of Advanced Types of Atherosclerotic Lesions and a Histological Classification of Atherosclerosis. *Arteriosclerosis, Thrombosis, and Vascular Biology* 1995, 9(15).
33. Whitman SC. A practical approach to using mice in atherosclerosis research. Clin Biochem Rev. 2004;25(1):81–93.
34. Guo C, Ma R, Liu X, Xia Y, Niu P, Ma J, Zhou X, Li Y, Sun Z. Silica nanoparticles induced endothelial apoptosis via endoplasmic reticulum stress-mitochondrial apoptotic signaling pathway. CHEMOSPHERE. 2018;210:183–92.
35. Guo C, Yang M, Jing L, Wang J, Yu Y, Li Y, Duan J, Zhou X, Li Y, Zwsun Ccmu. Edu. Cn Z. Amorphous silica nanoparticles trigger vascular endothelial cell injury through apoptosis and autophagy via reactive oxygen species-mediated MAPK/Bcl-2 and PI3K/Akt/mTOR signaling. INT J NANOMED. 2016;11:5257–76.
36. *INT J NANOMED* 2015:1463.

37. Wang W, Zeng C, Feng Y, Zhou F, Liao F, Liu Y, Feng S, Wang X. The size-dependent effects of silica nanoparticles on endothelial cell apoptosis through activating the p53-caspase pathway. ENVIRON POLLUT. 2018;233:218–25.
38. Napierska D, Quarck R, Thomassen LCJ, Lison D, Martens JA, Delcroix M, Nemery B, Hoet PH. Amorphous Silica Nanoparticles Promote Monocyte Adhesion to Human Endothelial Cells: Size-Dependent Effect. SMALL. 2013;9(3):430–8.
39. Guo C, Ma R, Liu X, Chen T, Li Y, Yu Y, Duan J, Zhou X, Li Y, Sun Z. Silica nanoparticles promote oxLDL-induced macrophage lipid accumulation and apoptosis via endoplasmic reticulum stress signaling. SCI TOTAL ENVIRON. 2018;631–632:570–9.
40. Feng L, Yang X, Liang S, Xu Q, Miller MR, Duan J, Sun Z. Silica nanoparticles trigger the vascular endothelial dysfunction and prethrombotic state via miR-451 directly regulating the IL6R signaling pathway. *PART FIBRE TOXICOL* 2019, 16(1).
41. Choi HY, Hafiane A, Schwertani A, Genest J. High-Density Lipoproteins: Biology, Epidemiology, and Clinical Management. CAN J CARDIOL. 2017;33(3):325–33.
42. Peng J, Luo F, Ruan G, Peng R, Li X. Hypertriglyceridemia and atherosclerosis. *LIPIDS HEALTH DIS* 2017, 16(1).
43. Borén J, Williams KJ. The central role of arterial retention of cholesterol-rich apolipoprotein-B-containing lipoproteins in the pathogenesis of atherosclerosis. CURR OPIN LIPIDOL. 2016;27(5):473–83.
44. Li R, Navab M, Pakbin P, Ning Z, Navab K, Hough G, Morgan TE, Finch CE, Araujo JA, Fogelman AM, et al. Ambient ultrafine particles alter lipid metabolism and HDL anti-oxidant capacity in LDLR-null mice. J LIPID RES. 2013;54(6):1608–15.
45. Duan J, Liang S, Feng L, Yu Y, Sun Z. Silica nanoparticles trigger hepatic lipid-metabolism disorder in vivo and in vitro. 2018, Volume 13:7303–7318.
46. Yan Z, Wang W, Wu Y, Wang W, Li B, Liang N, Wu W. Zinc oxide nanoparticle-induced atherosclerotic alterations in vitro and in vivo. 2017, Volume 12:4433–4442.
47. Yu X, Zhao X, Ze Y, Wang L, Liu D, Hong J, Xu B, Lin A, Zhang C, Zhao Y, et al. Changes of serum parameters of TiO2 nanoparticle-induced atherosclerosis in mice. J HAZARD MATER. 2014;280:364–71.
48. Tian Chen JHCC. Cardiovascular effects of pulmonary exposure to titanium dioxide nanoparticles in ApoE knockout mice. J NANOSCI NANOTECHNO. 2013;13:3214–22.
49. Kang GS, Gillespie PA, Gunnison A, Moreira AL, Tchou-Wong K, Chen L. Long-Term Inhalation Exposure to Nickel Nanoparticles Exacerbated Atherosclerosis in a Susceptible Mouse Model. ENVIRON HEALTH PERSP. 2011;119(2):176–81.
50. Zhao L, Zhu Y, Chen Z, Xu H, Zhou J, Tang S, Xu Z, Kong F, Li X, Zhang Y, et al. Cardiopulmonary effects induced by occupational exposure to titanium dioxide nanoparticles. NANOTOXICOLOGY. 2018;12(2):169–84.

51. Navarese EP, Robinson JG, Kowalewski M, Kolodziejczak M, Andreotti F, Bliden K, Tantry U, Kubica J, Raggi P, Gurbel PA. Association Between Baseline LDL-C Level and Total and Cardiovascular Mortality After LDL-C Lowering. JAMA. 2018;319(15):1566.
52. Li Z, Hulderman T, Salmen R, Chapman R, Leonard SS, Young S, Shvedova A, Luster MI, Simeonova PP. Cardiovascular Effects of Pulmonary Exposure to Single-Wall Carbon Nanotubes. ENVIRON HEALTH PERSP. 2007;115(3):377–82.
53. Zhu M, Wang B, Wang Y, Yuan L, Wang H, Wang M, Ouyang H, Chai Z, Feng W, Zhao Y. Endothelial dysfunction and inflammation induced by iron oxide nanoparticle exposure: Risk factors for early atherosclerosis. TOXICOL LETT. 2011;203(2):162–71.
54. Yang X, Shao H, Liu W, Gu W, Shu X, Mo Y, Chen X, Zhang Q, Jiang M. Endoplasmic reticulum stress and oxidative stress are involved in ZnO nanoparticle-induced hepatotoxicity. TOXICOL LETT. 2015;234(1):40–9.
55. Chen R, Huo L, Shi X, Bai R, Zhang Z, Zhao Y, Chang Y, Chen C. Endoplasmic Reticulum Stress Induced by Zinc Oxide Nanoparticles Is an Earlier Biomarker for Nanotoxicological Evaluation. ACS NANO. 2014;8(3):2562–74.
56. Huo L, Chen R, Zhao L, Shi X, Bai R, Long D, Chen F, Zhao Y, Chang Y, Chen C. Silver nanoparticles activate endoplasmic reticulum stress signaling pathway in cell and mouse models: The role in toxicity evaluation. BIOMATERIALS. 2015;61:307–15.
57. Yu K, Chang S, Park SJ, Lim J, Lee J, Yoon T, Kim J, Cho M. Titanium Dioxide Nanoparticles Induce Endoplasmic Reticulum Stress-Mediated Autophagic Cell Death via Mitochondria-Associated Endoplasmic Reticulum Membrane Disruption in Normal Lung Cells. PLOS ONE. 2015;10(6):e131208.
58. Park E, Choi D, Kim Y, Lee E, Song J, Cho M, Kim J, Kim S. Magnetic iron oxide nanoparticles induce autophagy preceding apoptosis through mitochondrial damage and ER stress in RAW264.7 cells. TOXICOL IN VITRO. 2014;28(8):1402–12.
59. Chen R, Huo L, Shi X, Bai R, Zhang Z, Zhao Y, Chang Y, Chen C. Endoplasmic Reticulum Stress Induced by Zinc Oxide Nanoparticles Is an Earlier Biomarker for Nanotoxicological Evaluation. ACS NANO. 2014;8(3):2562–74.
60. Zhou J, Lhoták S, Hilditch BA, Austin RC. Activation of the Unfolded Protein Response Occurs at All Stages of Atherosclerotic Lesion Development in Apolipoprotein E–Deficient Mice. *CIRCULATION* 2005, 111(14):1814–1821.
61. Sozen E, Ozer NK. Impact of high cholesterol and endoplasmic reticulum stress on metabolic diseases: An updated mini-review. REDOX BIOL. 2017;12:456–61.
62. Cao Y, Long J, Liu L, He T, Jiang L, Zhao C, Li Z. A review of endoplasmic reticulum (ER) stress and nanoparticle (NP) exposure. LIFE SCI. 2017;186:33–42.
63. Santos CX, Tanaka LY, Wosniak J, Laurindo FR. Mechanisms and implications of reactive oxygen species generation during the unfolded protein response: roles of endoplasmic reticulum

oxidoreductases, mitochondrial electron transport, and NADPH oxidase. Antioxid Redox Signal. 2009;11(10):2409–27.

64. Linton MF, Babaev VR, Huang J, Linton EF, Tao H, Yancey PG. Macrophage Apoptosis and Efferocytosis in the Pathogenesis of Atherosclerosis. CIRC J. 2016;80(11):2259–68.
65. Bobryshev YV, Ivanova EA, Chistiakov DA, Nikiforov NG, Orekhov AN. Macrophages and Their Role in Atherosclerosis: Pathophysiology and Transcriptome Analysis. *BIOMED RES INT* 2016, 2016:1–13.
66. Zhao C, Zhou Y, Liu L, Long J, Liu H, Li J, Cao Y. Lipid accumulation in multi-walled carbon nanotube-exposed HepG2 cells: Possible role of lipophagy pathway. FOOD CHEM TOXICOL. 2018;121:65–71.
67. Long J, Ma W, Yu Z, Liu H, Cao Y. Multi-walled carbon nanotubes (MWCNTs) promoted lipid accumulation in THP-1 macrophages through modulation of endoplasmic reticulum (ER) stress. NANOTOXICOLOGY. 2019;13(7):938–51.
68. Castilho G, Okuda LS, Pinto RS, Iborra RT, Nakandakare ER, Santos CX, Laurindo FR, Passarelli M. ER stress is associated with reduced ABCA-1 protein levels in macrophages treated with advanced glycated albumin – Reversal by a chemical chaperone. The International Journal of Biochemistry Cell Biology. 2012;44(7):1078–86.
69. Xu X, Lei T, Li W, Ou H. Enhanced cellular cholesterol efflux by naringenin is mediated through inhibiting endoplasmic reticulum stress - ATF6 activity in macrophages. Biochimica et Biophysica Acta (BBA) - Molecular Cell Biology of Lipids. 2019;1864(10):1472–82.
70. Yao S, Tian H, Miao C, Zhang D, Zhao L, Li Y, Yang N, Jiao P, Sang H, Guo S, et al. D4F alleviates macrophage-derived foam cell apoptosis by inhibiting CD36 expression and ER stress-CHOP pathway. J LIPID RES. 2015;56(4):836–47.
71. Oh J, Riek AE, Weng S, Petty M, Kim D, Colonna M, Cella M, Bernal-Mizrachi C. Endoplasmic Reticulum Stress Controls M2 Macrophage Differentiation and Foam Cell Formation. J BIOL CHEM. 2012;287(15):11629–41.
72. Yao S, Miao C, Tian H, Sang H, Yang N, Jiao P, Han J, Zong C, Qin S. Endoplasmic Reticulum Stress Promotes Macrophage-derived Foam Cell Formation by Up-regulating Cluster of Differentiation 36 (CD36) Expression. J BIOL CHEM. 2014;289(7):4032–42.
73. Kreider ML, Cyrs WD, Tosiano MA, Panko JM. Evaluation of Quantitative Exposure Assessment Method for Nanomaterials in Mixed Dust Environments: Application in Tire Manufacturing Facilities. ANN OCCUP HYG. 2015;59(9):1122–34.
74. Inoue K, Takano H. Aggravating Impact of Nanoparticles on Immune-Mediated Pulmonary Inflammation. The Scientific World JOURNAL. 2011;11:382–90.
75. Winkler-Heil R, Hofmann W. Modeling particle deposition in the Balb/c mouse respiratory tract. INHAL TOXICOL. 2016;28(4):180–91.
76. You R, Ho Y, Hung CH, Liu Y, Huang C, Chan H, Ho S, Lui S, Li H, Chang RC. Silica nanoparticles induce neurodegeneration-like changes in behavior, neuropathology, and affect synapse through MAPK activation. *PART FIBRE TOXICOL* 2018, 15(1).

77. Oh S, Kim B, Kim H. Comparison of nanoparticle exposures between fumed and sol-gel nano-silica manufacturing facilities. IND HEALTH. 2014;52(3):190–8.
78. Ji JH, Yu IJ. Estimation of human equivalent exposure from rat inhalation toxicity study of silver nanoparticles using multi-path particle dosimetry model. TOXICOL RES-UK. 2012;1(3):206.
79. FDA. Guidance for Industry-Estimating the Maximum Safe Starting Dose in Initial Clinical Trials for Therapeutics in Adult Healthy Volunteers.: U.S. Department of Health and Human Services-Food and Drug Administration-Center for Drug Evaluation and Research (CDER); 2005.
80. Ni M, Zhang M, Ding SF, Chen WQ, Zhang Y. Micro-ultrasound imaging assessment of carotid plaque characteristics in apolipoprotein-E knockout mice. ATHEROSCLEROSIS. 2008;197(1):64–71.
81. Daugherty A, Tall AR, Daemen MJAP, Falk E, Fisher EA, García-Cardeña G, Lusis AJ, Owens AP, Rosenfeld ME, Virmani R. Recommendation on Design, Execution, and Reporting of Animal Atherosclerosis Studies: A Scientific Statement From the American Heart Association. *CIRC RES* 2017, 121(6).

Figures

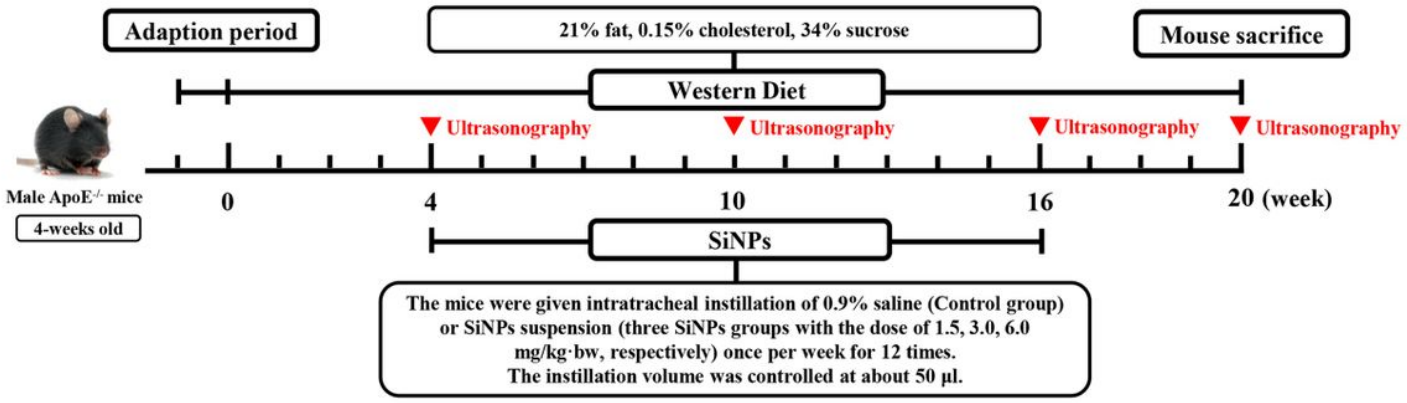

Figure 1

Experimental design of SiNPs promoted the atherosclerotic plaque progression in ApoE-/- mice. 4-weel-old male ApoE-/- mice fed a Western diet were exposed to SiNPs via intratracheal instillation for 12 times, once per week, in order to investigate the influence of sub-chronic SiNPs exposure on the development of atherosclerosis.

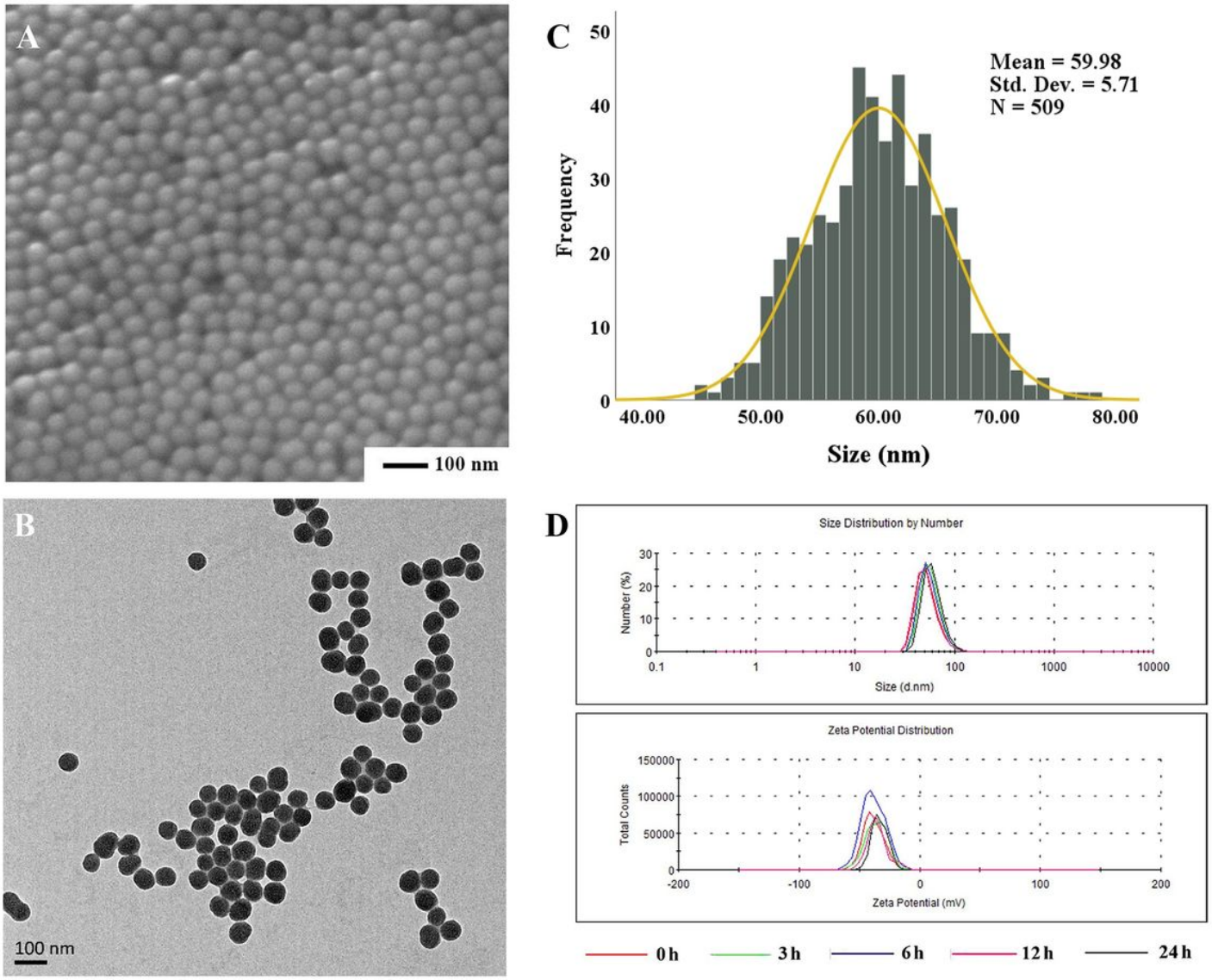

Figure 2

Characterization of SiNPs. Representative SEM (A) and TEM (B) images of SiNPs. Scale bar = 100 nm. (C) SiNPs are normally distributed with a mean diameter of 59.98 ± 5.71 nm. (D) The hydrodynamic size and zeta potential distribution of SiNPs in distilled water.

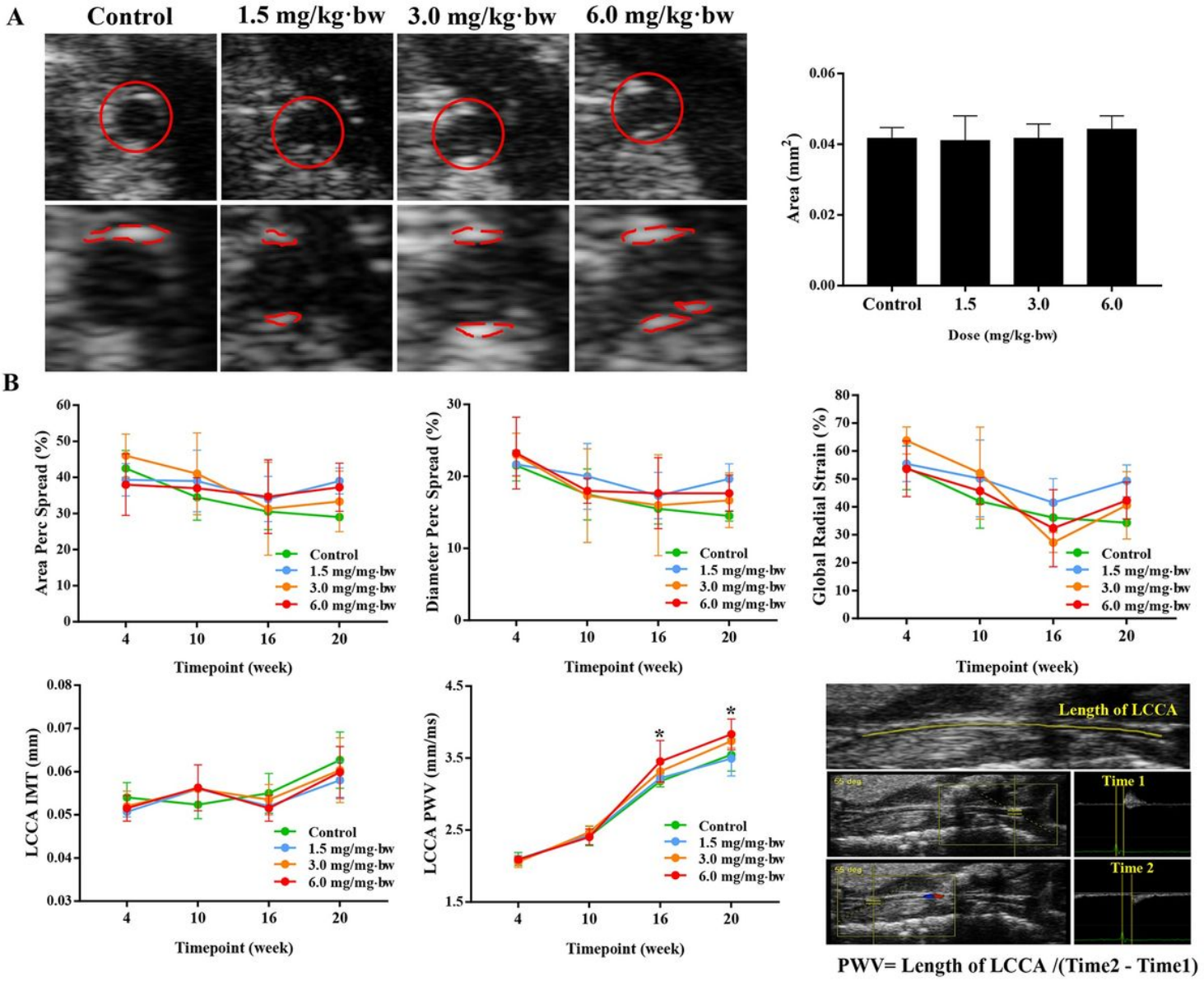

Figure 3

SiNPs promoted the stiffness of carotid artery in ApoE-/- mice. (A) Plaque in the left common carotid artery (LCCA) was captured by using ultrasonic biomicroscopy, and the plaque area was calculated at the end of the experiment. (B) The area percent spread, diameter percent spread, global radial strain, intima-media thickness (IMT) and pulse wave velocity (PWV) of the left common carotid artery (LCCA) were measured at different timepoints. *p < 0.05 vs Control group at the same timepoint. Data are expressed as means ± SD, n = 3.

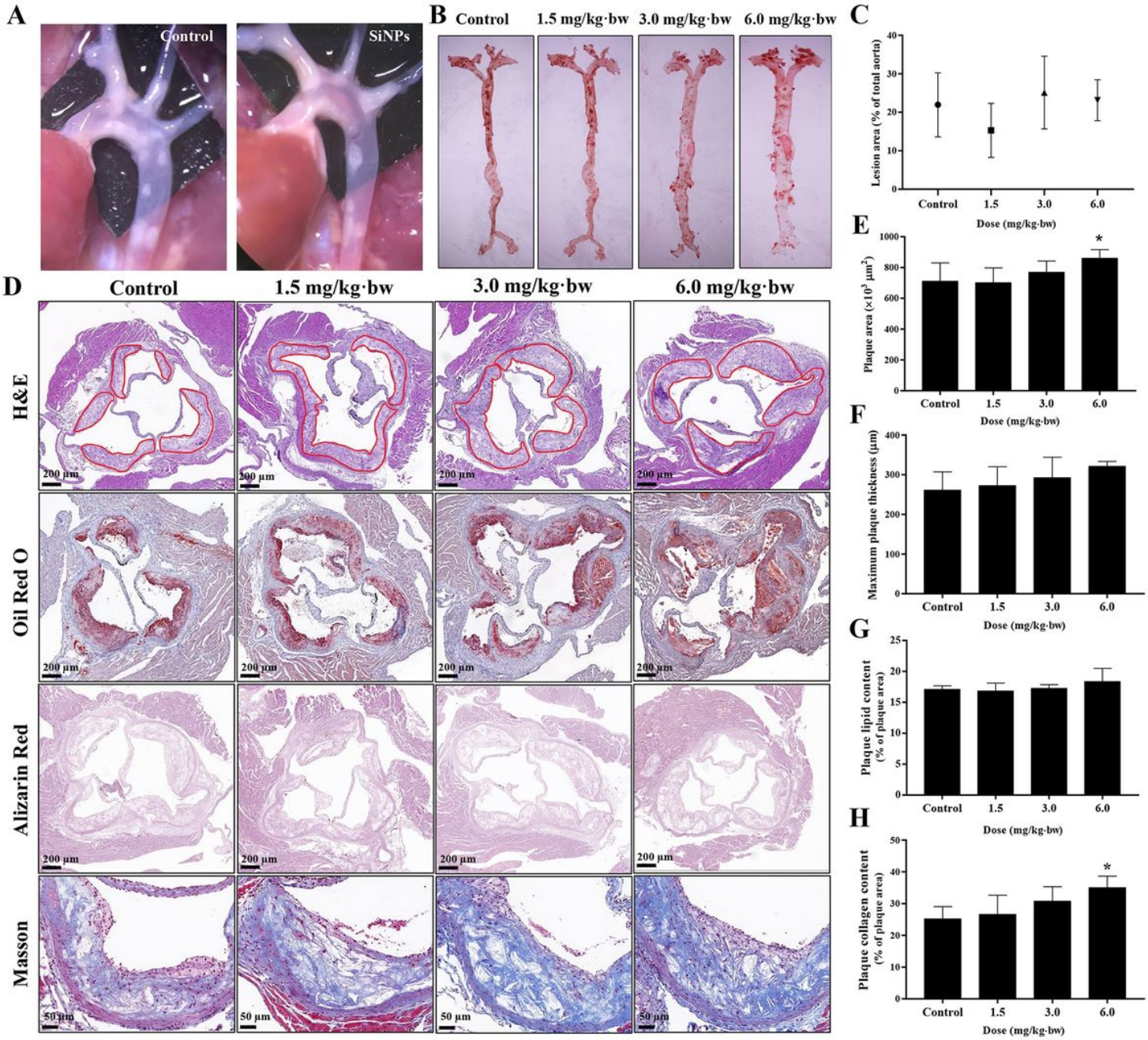

Figure 4

Effect of SiNPs on the progression of atherosclerosis. Representative images of a mouse aorta with atherosclerotic plaque (A), and the whole aorta stained by Oil red O was arranged for optimal measurement of lesion area by en-face analysis (B, C). n = 3. (D) Representative images of H&E, Oil Red O, Alizarin Red and Masson staining in aortic root. Scale bar = 200 μm or 50 μm. (E, F) The analysis of plaque area and maximum plaque thickness based on H&E staining, n = 6. (G) The plaque lipid content based on Oil Red O staining, n = 4. (H) Plaque collagen content based on Masson staining, n = 4. *p < 0.05 vs Control. Data are expressed as means ± SD.

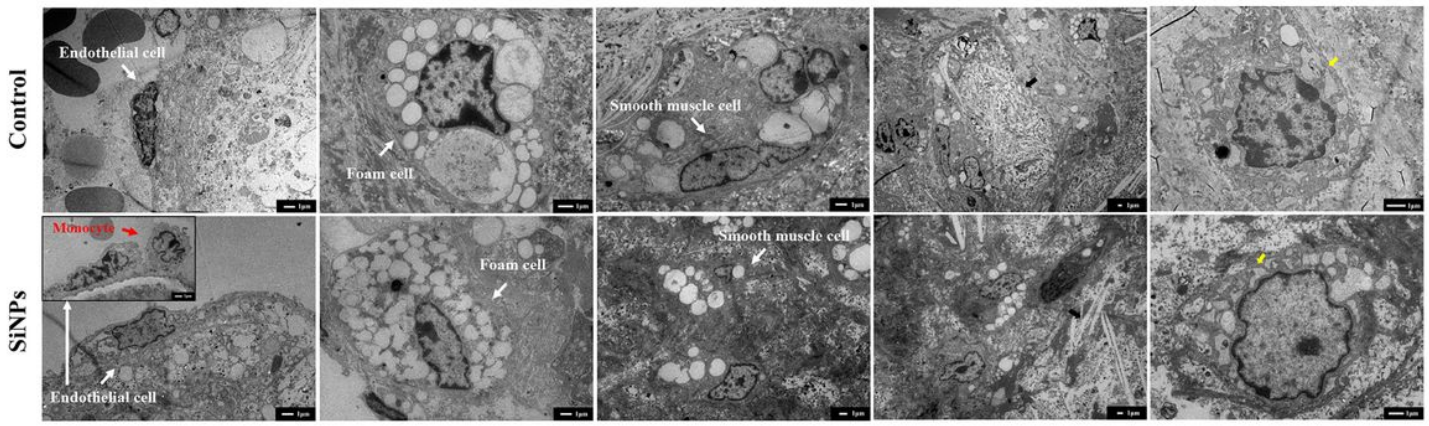

Figure 5

Representative TEM picture of the plaque. Foam cells, migrated smooth muscle cells, and a large amount of cholesterol crystals and necrotic substances (black arrow) were observed in the lesions of mice in control or SiNPs exposed group. The expansion of endoplasmic reticulum was observed within macrophages inside the lesion (yellow arrow). Scale bar = 1 μm.

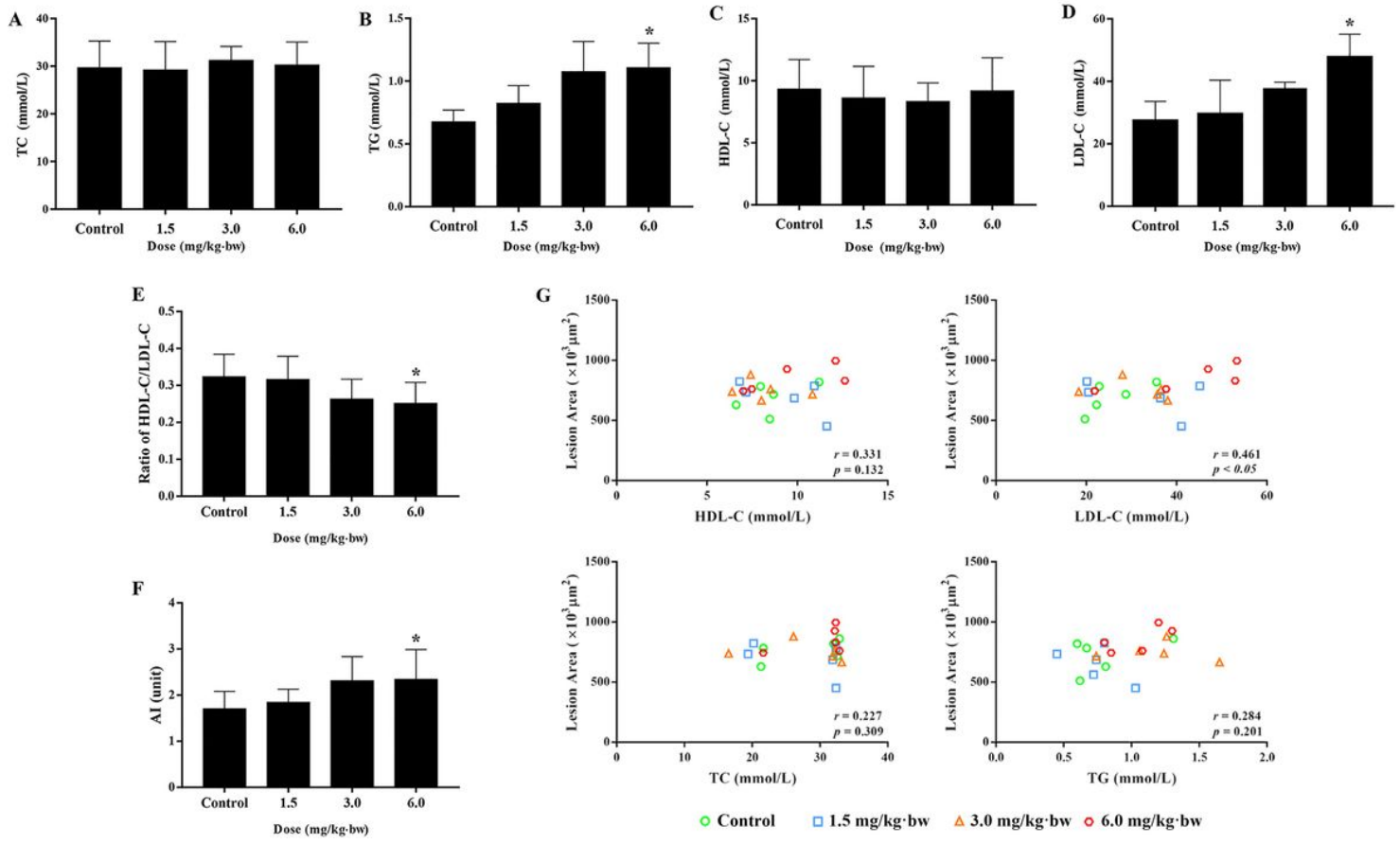

Figure 6

Effect of SiNPs on serum lipid profiles. The TC (A), TG (B), LDL-C (C), and HDL-C (D) were detected, and the ratio of HDL-C/LDL-C (E) and AI (F) were calculated. The correlation between serum TC, TG, LDL-C,

HDL-C content and aortic root plaque area was analyzed (G). r : Correlation coefficient, *p < 0.05 vs Control. Data are expressed as means ± SD, n = 6.

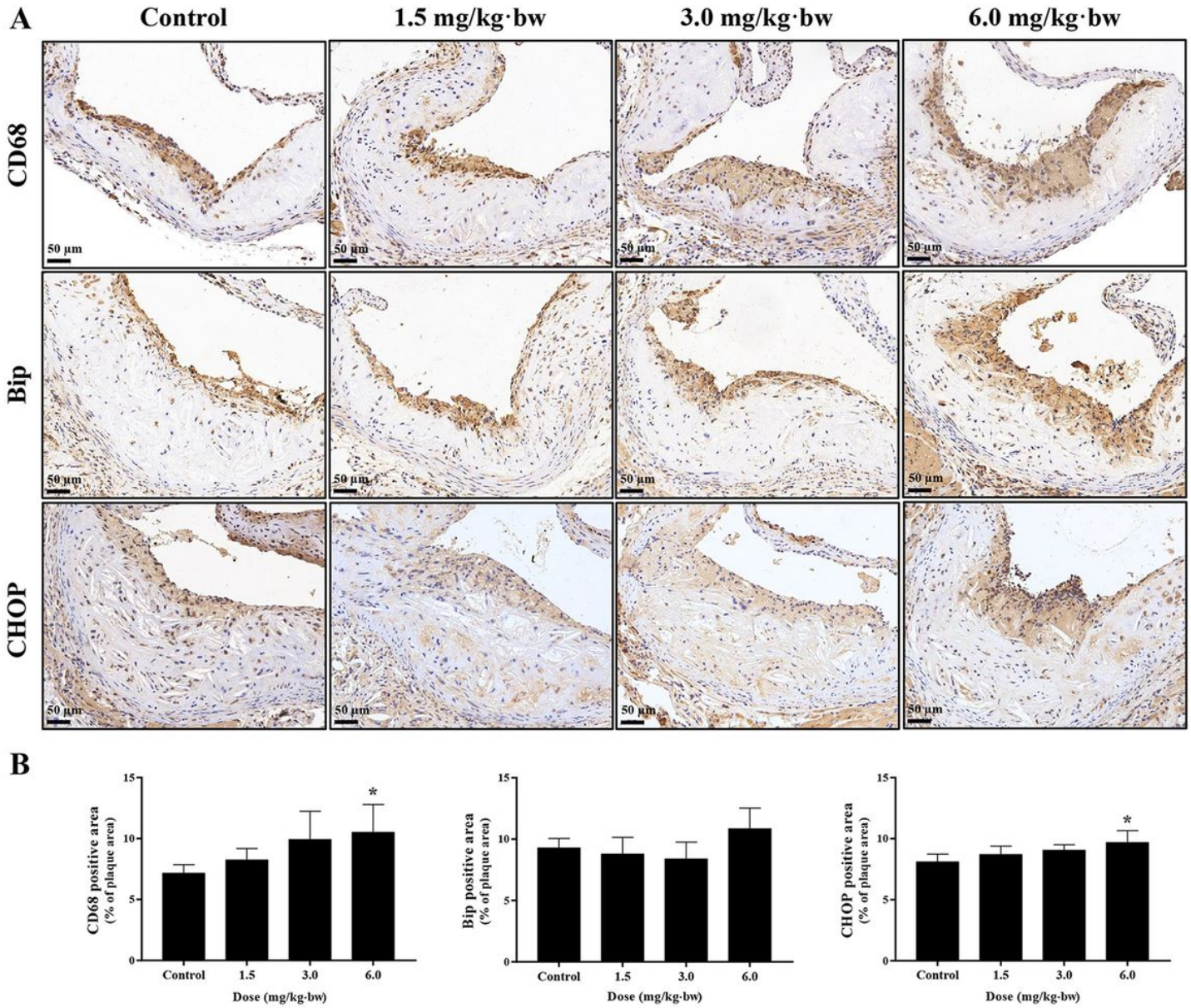

Figure 7

SiNPs activated ER stress in atherosclerotic lesion. (A) Representative images of immunohistochemistry staining of CD68, Bip and CHOP in aortic roots. Scale bar = 50 μm. (B) Statistical analyses of CD68-, Bip-, CHOP- positive area in aortic roots. n = 4. *p < 0.05 vs Control. Data are expressed as means ± SD.

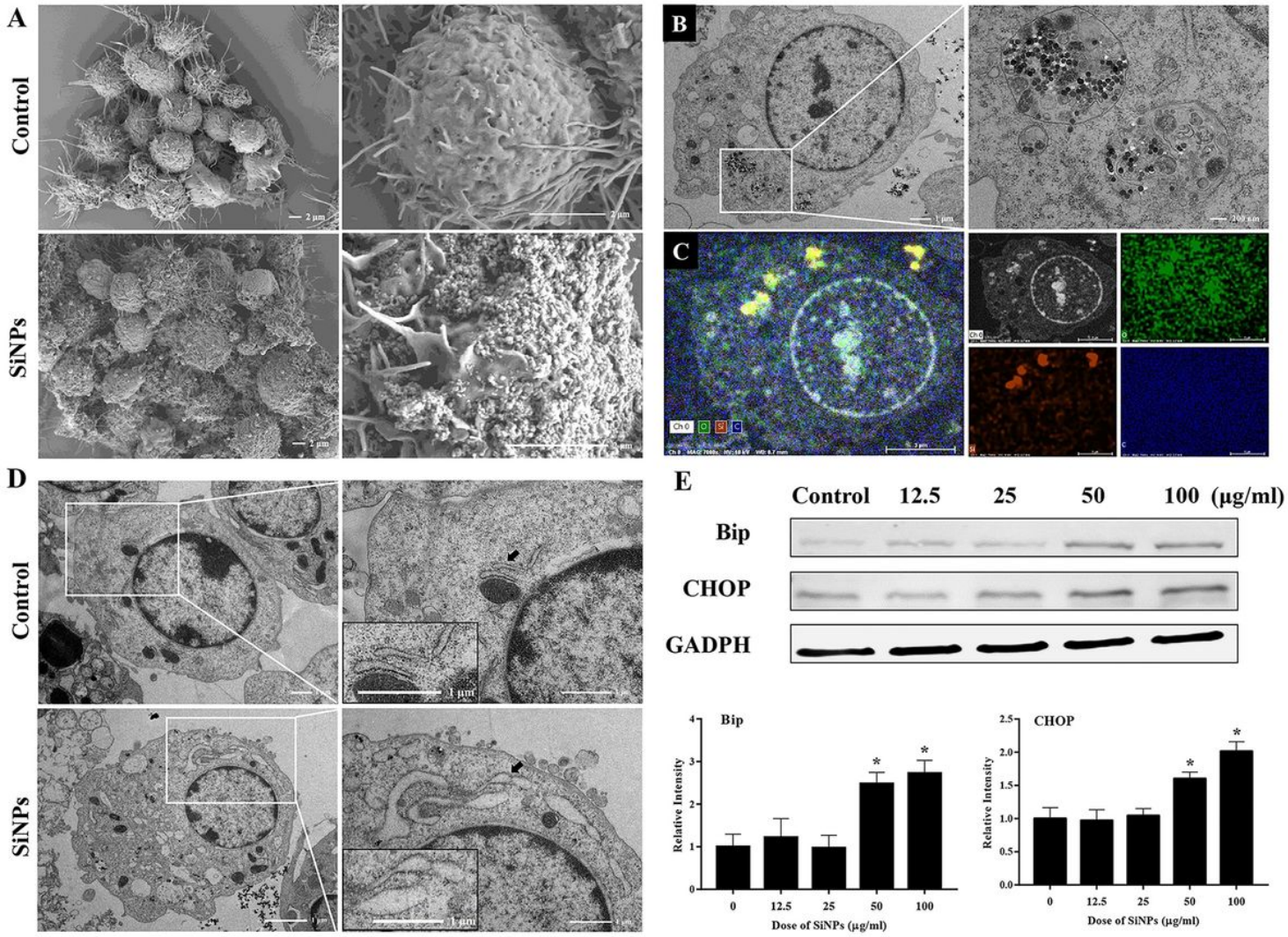

Figure 8

SiNPs were internalized and activated ER stress in RAW264.7 cells. The cells were treated with 50 μg/ml SiNPs for 24 hours. Representative images of SEM (A) and TEM (B) respectively indicated the visualization of particle aggregates on the cellular surface, and uptake in macrophage after SiNPs treatment. Scale bar = 200 nm, 1 or 2 μm. (C)The uptake of SiNPs was further measured by energy dispersive spectrometry. In coincidence with the TEM image, silicon (red) and oxygen (green) element were detected. Scale bar = 3 μm. (D) Representative TEM images indicated ER stress as evidenced by ER expansion and degranulation (black arrow). Scale bar = 1 μm. (E) The expressions of ER stress indicators, Bip and CHOP were detected by Western blot and the densitometric analysis was performed. *p < 0.05 vs Control. Data are expressed as means ± SD of three independent experiments.

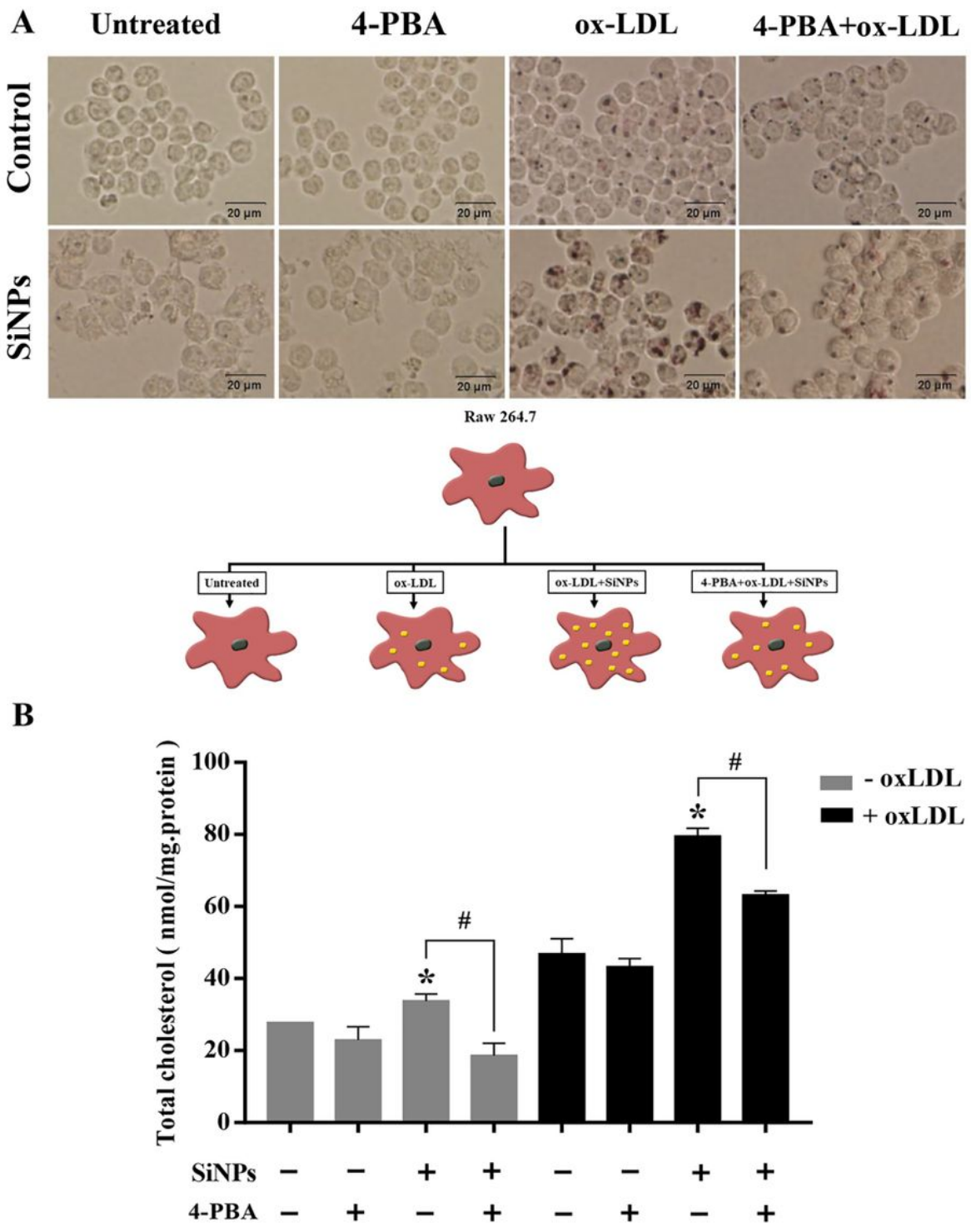

Figure 9

ER stress involved in the lipid accumulation induced by SiNPs in RAW264.7 cells. (A) Representative lipid droplet staining images by Oil Red O staining. Scale bar = 20μm. (B) The intracellular total cholesterol content of RAW264.7 cells. *p < 0.05 vs Control, #p < 0.05 vs SiNPs group with or without ox-LDL. Data are expressed as means ± SD of three independent experiments.

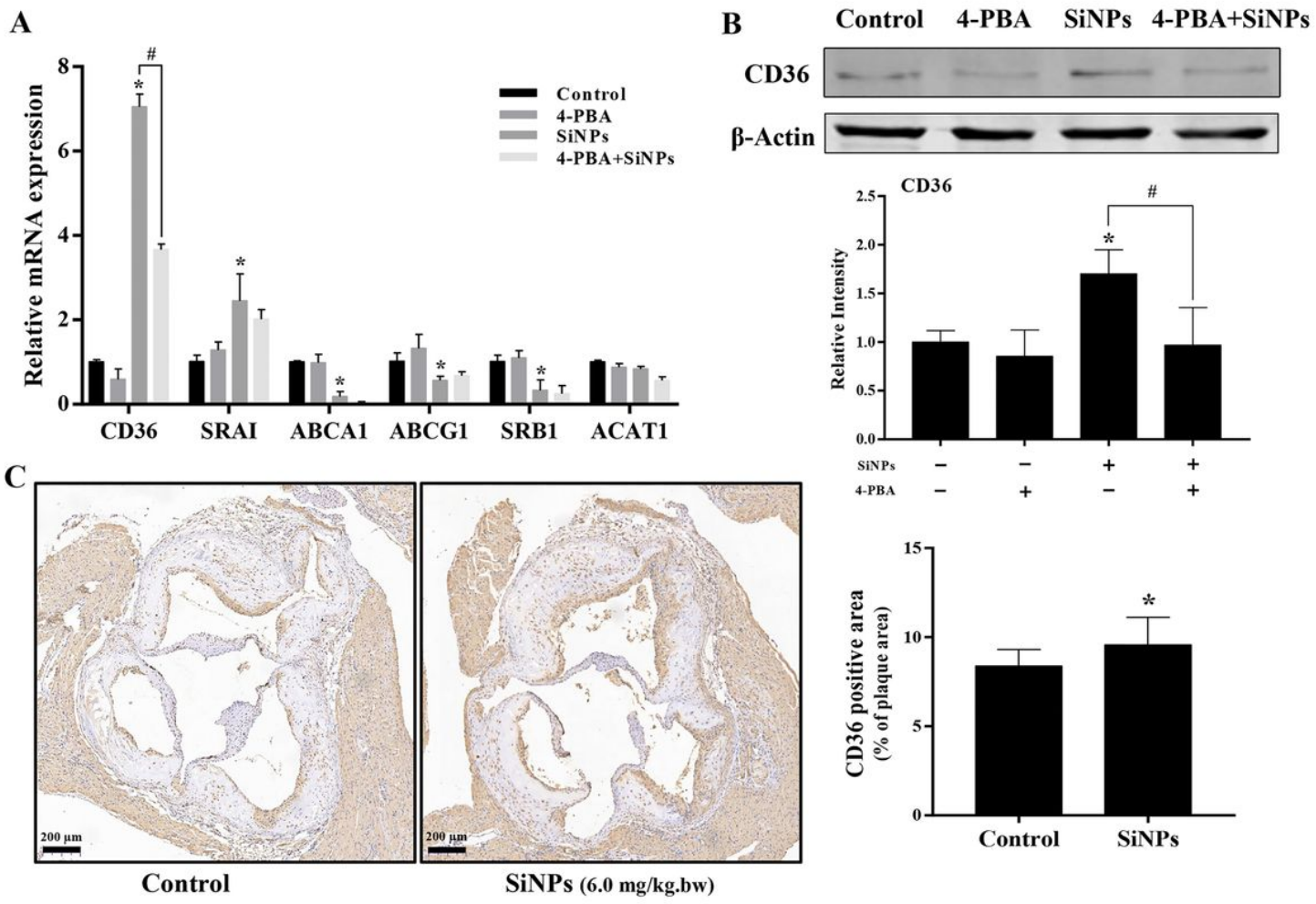

Figure 10

ER stress-mediated the up-regulated CD36 expression attributing to the lipid accumulation induced by SiNPs in RAW264.7cells. (A) The relative mRNA expressions of factors involved in cholesterol influx/efflux. (B) The CD36 protein expression of RAW264.7 cells. In consistent with the mRNA level, the up-regulated CD36 expression induced by SiNPs was greatly alleviated by 4-PBA pretreatment. Also, the CD36 expression in the plaque of SiNPs-exposed aortic root was up-regualted (C, n = 4). *p < 0.05 vs Control, #p < 0.05 vs SiNPs group. Data are expressed as means ± SD of three independent experiments.

Supplementary Files

This is a list of supplementary files associated with this preprint. Click to download.

- graphicabstract.jpg
- Supplementarymaterial.pdf